SCIENTIFIC REPORTS

OPEN

SUBJECT AREAS:
SOLAR CELLS
ELECTRON TRANSFER

Received
28 January 2014

Accepted
2 April 2014

Published
23 April 2014

p-type Mesoscopic Nickel Oxide/ Organometallic Perovskite Heterojunction Solar Cells

Kuo-Chin Wang[1], Jun-Yuan Jeng[1], Po-Shen Shen[1], Yu-Cheng Chang[2], Eric Wei-Guang Diau[2], Cheng-Hung Tsai[1], Tzu-Yang Chao[1], Hsu-Cheng Hsu[1], Pei-Ying Lin[1], Peter Chen[1,3,4], Tzung-Fang Guo[1,3,4] & Ten-Chin Wen[5]

[1]Department of Photonics, National Cheng Kung University, Tainan, Taiwan 701, [2]Department of Applied Chemistry and Institute of Molecular Science, National Chiao Tung University, Hsinchu, Taiwan 300, [3]Advanced Optoelectronic Technology Center (AOTC), [4]Research Center for Energy Technology and Strategy (RCETS), [5]Department of Chemical Engineering National Cheng Kung University, Tainan, Taiwan 701.

Correspondence and requests for materials should be addressed to P.C. (petercyc@mail.ncku.edu.tw) or T.F.G. (guotf@mail.ncku.edu.tw)

In this article, we present a new paradigm for organometallic hybrid perovskite solar cell using NiO inorganic metal oxide nanocrystalline as p-type electrode material and realized the first mesoscopic NiO/perovskite/[6,6]-phenyl C61-butyric acid methyl ester ($PC_{61}BM$) heterojunction photovoltaic device. The photo-induced transient absorption spectroscopy results verified that the architecture is an effective p-type sensitized junction, which is the first inorganic p-type, metal oxide contact material for perovskite-based solar cell. Power conversion efficiency of 9.51% was achieved under AM 1.5 G illumination, which significantly surpassed the reported conventional p-type dye-sensitized solar cells. The replacement of the organic hole transport materials by a p-type metal oxide has the advantages to provide robust device architecture for further development of all-inorganic perovskite-based thin-film solar cells and tandem photovoltaics.

Organometallic perovskite materials have been studied intensively since the pioneer work delivered by Kojima et al. which demonstrated that the organic-inorganic hybrid perovskite behaved like a light harvester[1]. Successive report by Park's group showed improved performance based on the similar liquid dye-solar-cell like device[2]. Until the breakthrough by the introduction of solid organic hole conductor to replace the liquid electrolyte, the new perovskite-type solar cells achieved remarkable efficiency and attracted enormous attention[3,4]. Since then, massive research works using various contact materials and device configurations, evolved from dye-sensitized solar cells (DSCs) with mesocsopic or super-mesoscopic structure and extreme thin absorber (ETA) structure, to organic photovoltaics (OPVs) with a planar heterojunction (PHJ), have emerged during the past few years[5–10]. Recent progresses with 15% power conversion efficiency (PCE) in either a mesoscopic or a PHJ have demonstrated that this organic-inorganic hybrid perovskite material is one of the most promising candidates for cost effective solar absorber in the future[11–13]. Efficiency exceeding 20% might be realized by further optimization through fill factor improvement and tandem architecture with multiple solar cells[6,14]. The beauty of perovskite material is the diversity in its device architectures due to the distinct material properties such as broad absorption spectra range with high extinction coefficient, ambipolar diffusion, and long carrier diffusion length[15–17]. These merits allow the organic-inorganic hybrid perovskite being a light absorber superior to those of the solution-based photovoltaic such as DSCs, OPVs or other thin-film photovoltaics.

In addition, the voltage output of perovskite-based solar cells is relatively high among the other solution-processed photovoltaics mainly due to the minimized intrinsic potential losses that are inevitable for interfacial charge transfer in DSCs and the cost of exciton dissociation energy in OPVs. Open-circuit voltage (V_{oc}) more than 1 volt, which is close to the inherent thermodynamic limit, has been demonstrated in many reports[8,12,13,18,19]. Currently the most successful device configuration is the junction (either mesoscopic or PHJ) with a n-type metal oxide/perovskite/hole transport materials (HTMs) where the metal oxide layer and the organic HTM act as selective contacts to facilitate charge extraction[11–13,20,21]. Another inverse structure, using non-oxide n-type material as electron acceptor composed of poly(3,4-ethylenedioxythiophene) poly(styrenesulfonate) (PEDOT:PSS)/perovskite/fullerene planar junction, has been demonstrated with great success and remarkable conversion efficiency recently[7–9,22]. This OPV-like sandwich bilyaer junction structure has great potential for low

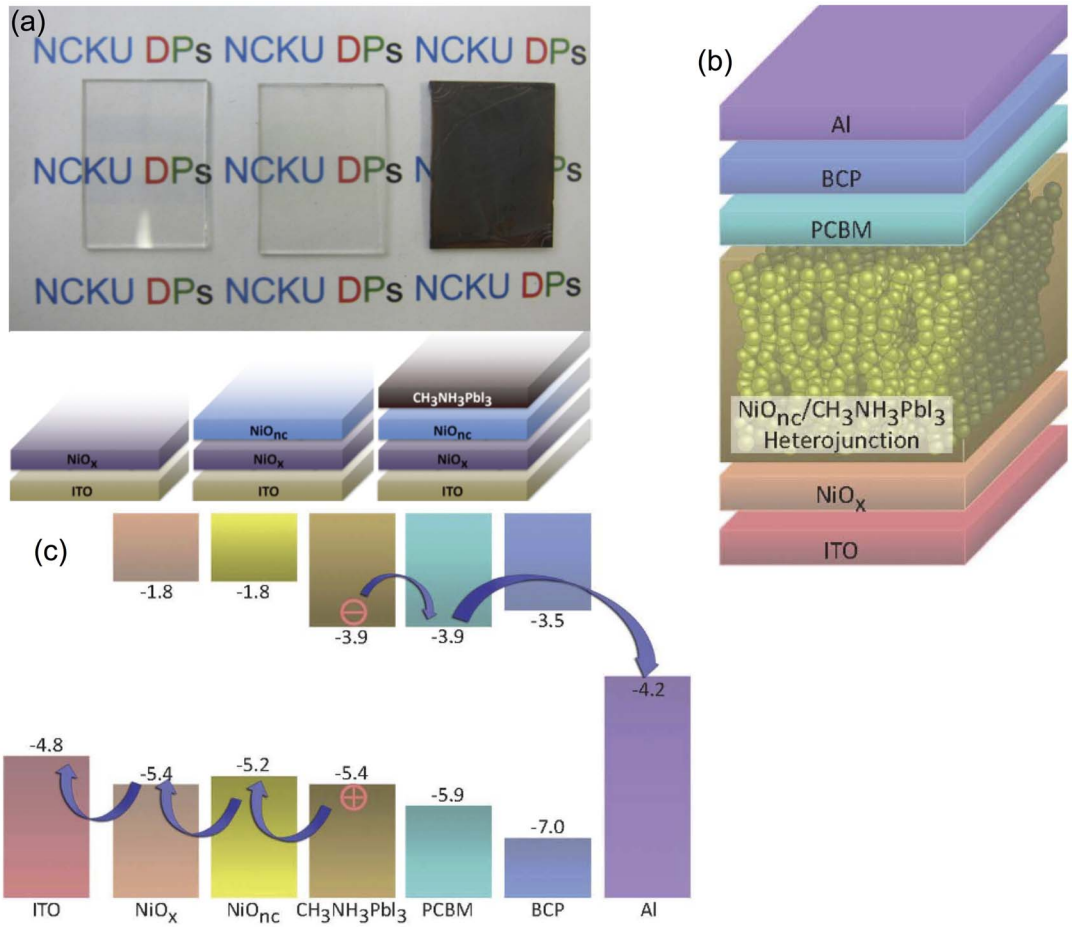

Figure 1 | (a) The photos and illustrations of patterned ITO glass, ITO glass with NiO_x thin film and mesoscopic NiO_{nc} with perovskite coated electrode. (b) The schematic of the whole device. (c) The energy level diagram of the mesoscopic NiO_{nc}/perovskite/PCBM heterojunction.

temperature process and flexible devices[8,13,22]. A basic photovoltaic device is the sandwich of light absorbing materials between effective selective contacts. For perovskite absorber, the most commonly used n-contacts are TiO_2[3,11,12,23–26], ZnO[13,19,27], fullerene derivatives[7–9] while the successful p-contacts are mostly organic materials such as 2,2′, 7,7′-tetrakis(N,N-di-p-methoxyphenylamino)-9,9′- spirobifluorene (Spiro-OMeTAD) or other hole transporting materials (like poly-3-hexylthiophene (P3HT) or poly-triarylamine derivative)[18,22,28–33]. Recently, perovskite-based cell using CuI inorganic p-type semiconductor as hole transport layer delivered 6% efficiency has been reported[34]. Mainly due to the unfavorable energy level match between the valence band of CuI and perovskite, the voltage was considerably reduced compared to most of the highly efficient perovskite solar cells. However, this research highlighted the direction to develop all-inorganic materials for perovskite-based photovoltaic devices.

NiO has been one of the rarely successful candidates as p-type contact material for OPVs and DSCs[35–42]. Since organometallic perovskite has showed amibipoar charge transport behavior, sensitization of p-type wide band gap oxide shall be a feasible approach as the conventional n-type sensitization concept. Thus, we constructed the heterojunction solar cells with a p-i-n active layer composed of the mesoscopic NiO/peroskite/[6,6]-phenyl C61-butyric acid methyl ester ($PC_{61}BM$) structure. In this report, we realized a highly efficient (9.51%) mesoscopic NiO/perovskite junction where the p-contact is replaced with mesoscopic inorganic metal oxide material to feature efficient charge separation in the NiO/perovskite interface. The success of efficient p-type sensitization or heterojunction solar cells is critical for the future design of tandem devices or p-n dual-sensitization configuration in the future[36].

The details for the experimental procedures are described in the Methods section. The images of devices after NiO_x thin film, NiO nanocrystalline (NiO_{nc}) and perovskite deposition are illustrated in Fig. 1(a). The substrate coated with NiO_x/NiO_{nc} remained optically transparent with certain absorption in the range of 400 ~ 450 nm (See Supplementary Fig. 1S for transmission spectra). After the perovskite is deployed into the mesoscopic electrode, the device turned dark brown as shown in the right photo on Fig. 1(a). The full device structure is shown in Fig. 1(b) with the energy level of the each material illustrated in Fig. 1(c). The energy level of NiO_x was taken from our previous study which the valance band was determined by ultraviolet photoelectron spectroscopy (UPS)[43]. The energy level for the NiO nanoparticle was given from the literature reported by Powar et al. where the valence band edge of NiO was measured using photoelectron spectroscopy in air (PESA)[37]. The ideal energy levels of the lowest unoccupied molecular orbital (LUMO) of $PC_{61}BM$ and valence band edge of NiO are located in the vicinity of the band edges of perovskite. This arrangement is appropriate for receiving high voltage with minimum loss providing the charge separation process between the absorber and selective contacts is efficient. The scanning electron microscopy (SEM) images of the corresponding illustrations in Fig. 1(a) are shown in Fig. 2. The NiO_x thin film is very compact without pinholes or crevices as seen in Fig. 2(a). In Fig. 2(b), the NiO nanocrystalline showed feature sizes around few tenths of nanometers. Some aggregates above 100 nm are observed due to incomplete dispersion. We perceived Fig. 2(c) the filling of perovskite

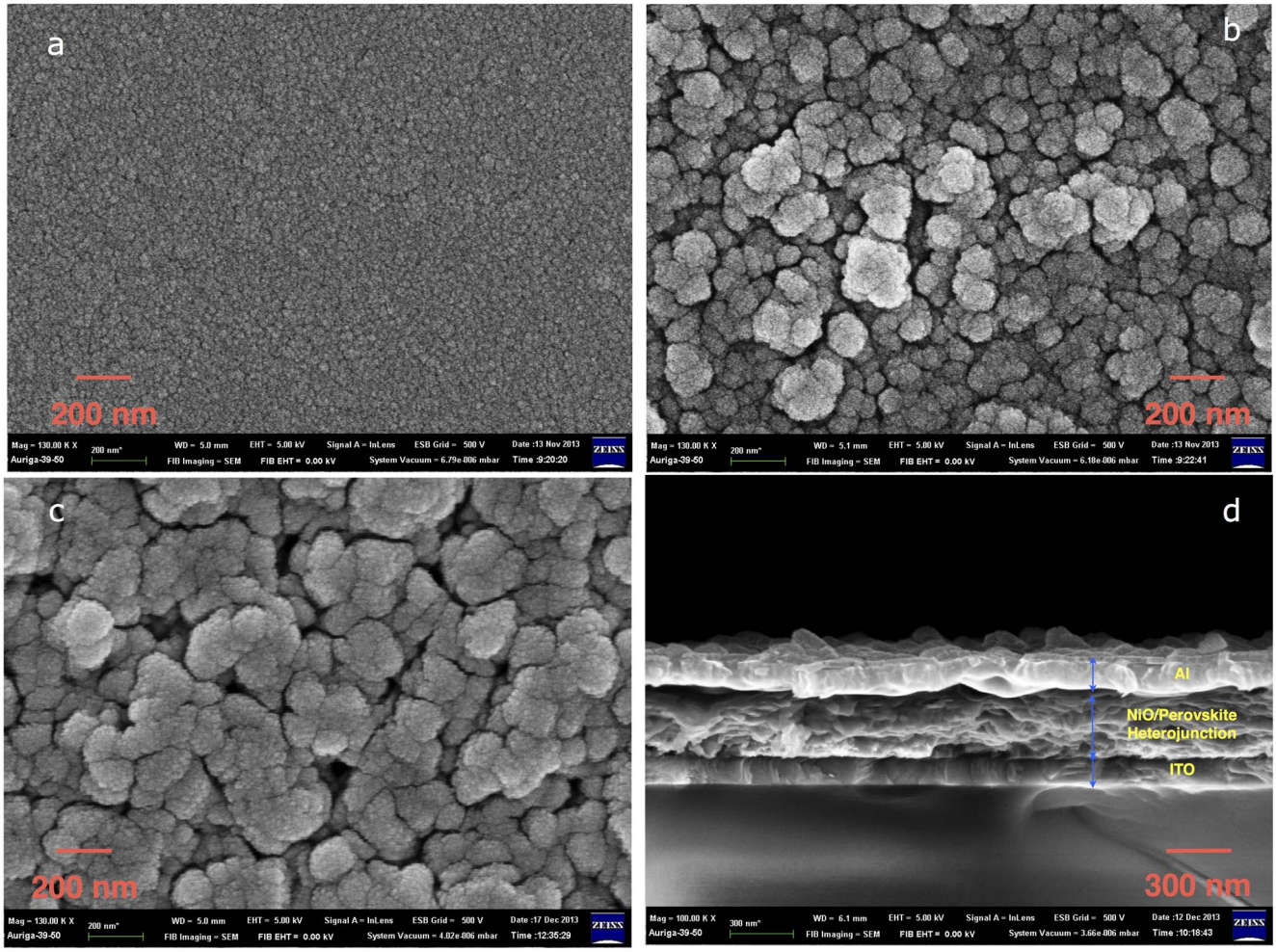

Figure 2 | Top view SEM images of (a) NiO_x thin film, (b) NiO_{nc} nanocrystalline, (c) perovskite coated on (b). (d) The cross sectional image of the whole device. The magnification in (a, b, c) is 130,000 with the scale bar of 200 nm, while the magnification in (d) is 100,000 with scale bar of 300 nm.

nanocrystals on the mesoscopic porous NiO_{nc} network after sequential deposition of PbI_2 and CH_3NH_3I with relative conformal coating leaving some small pores between the particles. It seems that no thick perovskite overlayer is formed on top of the NiO_{nc} porous film, which suggests the role of $PC_{61}BM$ and bathocuproine (BCP) coating is critical for making good contact with the subsequent metal electrode. The cross sectional SEM image of the full device is presented in Fig. 2(d) showing the active mesoscopic NiO_{nc}/perovskite layer is around 250 nm.

The current-voltage characteristics are presented in Fig. 3(a) with their corresponding incident photon to electron conversion efficiency (IPCE) in Fig. 3(b) and photovoltaic parameters listed in Table 1. The best-performing cell using $PC_{61}BM$ delivered high V_{oc} of 1040 mV with short-circuit photocurrent density (J_{sc}) of 13.24 mA/cm^2 and 69% fill factor, leading to an overall PCE of 9.51%. Another device using [6,6]-phenyl C71-butyric acid methyl ester ($PC_{71}BM$) obtained very similar photovoltaic performance with V_{oc} of 1000 mV, J_{sc} of 14.65 mA/cm^2 and fill factor of 64%, resulted in an overall PCE of 9.44%. The effects of these two fullerene derivatives on their photovoltaic performances are very similar to what previously reported in OPV, which the device composed of $PC_{71}BM$ acceptor has slightly blue-shifted IPCE with lower voltage and higher current characteristics[44–47]. Whether the absorption of $PC_{71}BM$ between 400 ~ 600 nm has contribution to the photocurrent remained unclear and further investigations are in progress to understand this phenomenon. However, the thickness of the $PC_{61}BM$ or $PC_{71}BM$ layer was extremely thin (20 ~ 25 nm) in our device so that the differences in current response is relatively minor compared to those of OPVs. The cut-off of the IPCE below 450 nm is due to the absorption of NiO_x/NiO_{nc} which filtered the transmission of incident light[35]. Transmission of indium tin oxide (ITO glass) coated with NiO_x/NiO_{nc} is given in supplemental information (Fig. S1). The high V_{oc} received from the junction demonstrated the advantage of energy level alignment between light absorber and the selective contacts. This extraordinary voltage output is a distinct characteristic for all the highly efficient perovskite-based photovoltaic devices[11–13,22]. The energy loss in charge extraction is minimized by using $PC_{61}BM$ whose LUMO is nearly identical with the conduction band edge of perovskite while the NiO_{nc} valance band is close to that of perovskite.

To elucidate the effect of the mesoscopic structure, a flat electrode of oxide ITO/NiO_x (without the NiO nanocrystalline layer) was applied for comparison. The flat junction cell delivered PCE of 7.40% (green line in Fig. 3 (a)) which is consistent with our previous report on the PHJ perovskite/fullerene solar cells[43]. The implement of mesoscopic NiO layer provided an increased film thickness to host the light absorbing perovskite material and prevented the risk of morphological defect that deteriorate the photovoltaic function. The improved photovoltaic performances of the mesoscopic devices are obvious and mainly due to the slightly increased current and voltage with respect to the PHJ cell. We attributed this phenomenon to the better morphological formation of perovskite in mesoscopic electrode compared with that of NiO_x. In our previous work, we have found that the V_{oc} for the PHJ devices is influenced by the work function of electrode interlayer, the spin speed of perovskite coating

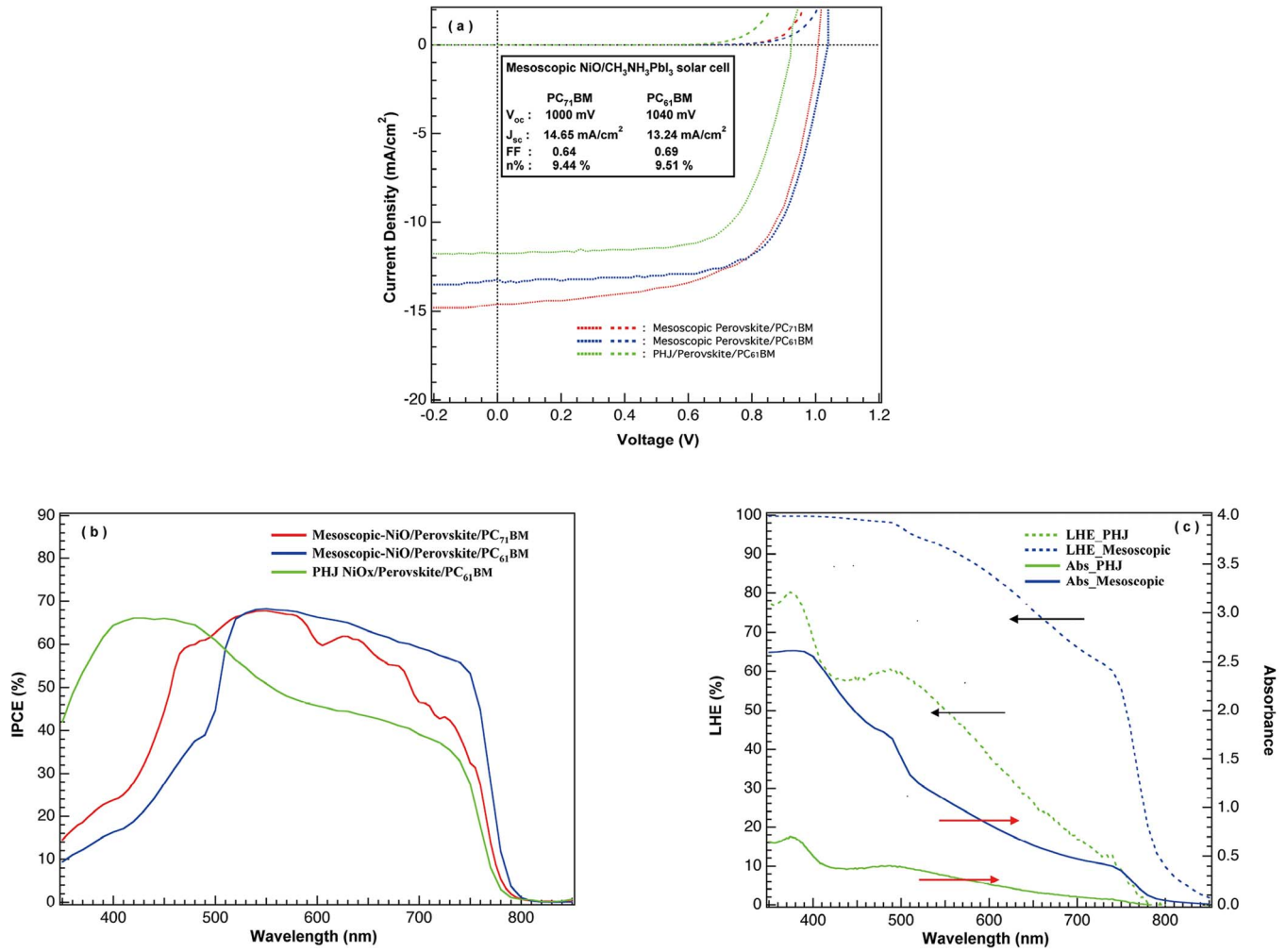

Figure 3 | (a) The current-voltage characteristics of photovoltaic devices made of mesoscopic NiO_{nc}/perovskite/PCBM hetrojunction solar cell (red line for $PC_{71}BM$ and blue line for $PC_{61}BM$) and planar NiO_x/perovskite/$PC_{61}BM$ heterojunction solar cells (green line). (b) The IPCE of mesoscopic NiO_{nc}/perovskite/$PC_{71}BM$ device (red line), mesoscopic NiO/perovskite/$PC_{61}BM$ device (blue line) and planar NiO_x/perovskite/$PC_{61}BM$ heterojunction solar cell (green line). (C) The light harvesting efficiency (LHE) and absorbance of mesoscopic NiO_{nc}/perovskite film (blue dot and blue line), and planar NiO_x/perovskite film (green dot and green line).

and surface morphology[43]. The SEM images of perovskite coated with various deposition conditions on the planar NiO_x are available in literature[43]. One image of the perovskite thin film spin coated with 9500 rpm on NiO_x for the PHJ device applied in this article is presented in Figure S2. Some small voids are presented on the surface which could impair the photovoltaic performance (mainly V_{oc}) due to internal shunt between the selective contact thin film in the PHJ device. When a mesoscopic electrode is applied as charge (hole) collector, it is expected that the sequential deposition method provides better filling of perovskite into the nano-porous pore and more conformal surface coverage on the NiO_{nc} surface which prevent direct contact between the n-contact layer (PCBM) with the p-contact materials (NiO_{nc} or NiO_x) This thin overlayer capping of perovskite on the NiO_{nc} is advantageous for the voltage. Another difference between mesoscopic and PHJ devices is the amount of perovskite loading on the substrate ending up with more light harvesting efficiency (LHE) in the mesoscopic junction device than for the PHJ device. The measured absorbance and calculated LHE ($LHE=1\text{-}10^{-A}$) are presented in Fig. 3 (c) where we find a nearly saturated LHE for the layer of perovskite coated on the mesoscopic NiO_{nc} thin film. The transmission loss is not significant in the PHJ device without the presence of NO_{nc} layer as we can observe from the IPCE in Fig. 3(b) where the quantum conversion efficiency at the short wavelength region (400 ~ 500 nm) remained high. The IPCE of the PHJ device basically follows the LHE curve shown in Fig. 3(c). On the other hand, the mesoscopic device received enhanced IPCE on the long wavelength due to the improved optical density from perovskite loading. In the actual device, the reflection of the back electrode (Al in this case) has to be taken into account for the optical process in the photoactive layer. For both the PHJ and the mesoscopic devices, the transmitted flux in the red part will be scattered back into the absorber thus resulted in an increased optical path and improved IPCE. This is the reason that the IPCE of PHJ is higher than the LHE in the long wavelength region. Meanwhile, we do observe an increased IPCE response in the red part for the mesoscopic cells compared with the PHJ cells[7,43]. From the LHE in Fig. 3(c) and the cross sectional SEM image shown in Fig. 2(d), the mesoscopic junction is about 250 nm which is thick enough to absorb 90% of the incident light. The IPCE of these two devices seem to be lower than the state-of-the-art devices. We believe that there are still some charge collection losses in the NiO/perovskite mesoscopic junction. The fill factor of 64 ~ 69% has not yet reached an optimized value. Further improvements on the material quality of NiO with better crystallinity, smaller particle size and well-dispersed mesoporous nanostructure are expected to promote the overall photovoltaic performance (especially the current) of this p-type oxide/perovskite

Table 1 | The photovoltaic parameters of mesoscopic and planar heterojunction NiO/perovskite solar cells. Their IV characteristic curves and IPCE responses are illustrated in Figure 3 (a) and (b) respectively

Device	Voltage (mV)	Current Density (mA/cm^2)	FF	Efficiency (%)
Mesoscopic NiO_{nc}/Perovskite/$PC_{71}BM$	1000	14.65	0.64	9.44
Mesoscopic NiO_{nc}/Perovskite/$PC_{61}BM$	1040	13.24	0.69	9.51
Planar NiOx/Perovskite/$PC_{61}BM$	920	11.77	0.68	7.40

heterojunction device. Using chloride-containing perovskite ($CH_3NH_3PbI_{3-x}Cl_x$) that has been reported with longer carrier diffusion length might be another approach to achieve higher efficiency[15]. Concerning the reproducibility for this type of device, statistic histogram on the photovoltaic parameters for 62 devices are summarized in supplemental information Fig. S3.

The key question for this newly developed NiO/perovskite junction is whether the holes in the photoexcited perovskite transfer into the NiO particles or the mesoscopic network only acts as a scaffold like the Al_2O_3 meso-superstructured solar cell[4]. Our previous photoluminescence (PL) spectra results demonstrated that NiO_x is capable of quenching the PL of perovskite[43]. To scrutinize the quenching process of perovskite by NiO_{nc}, the PL spectrum of NiO_{nc}/perovskite thin film used in the current study is shown in Fig. 4(a) in comparison with a reference of mesoscopic Al_2O_3 nanoparticles ($Al_2O_{3(nc)}$)/perovskite thin film. We observed strong quenching prevailed with the NiO_{nc}/perovskite sample, which implied charge transfer occurred at the NiO_{nc}/perovskite interface. PL has been applied to

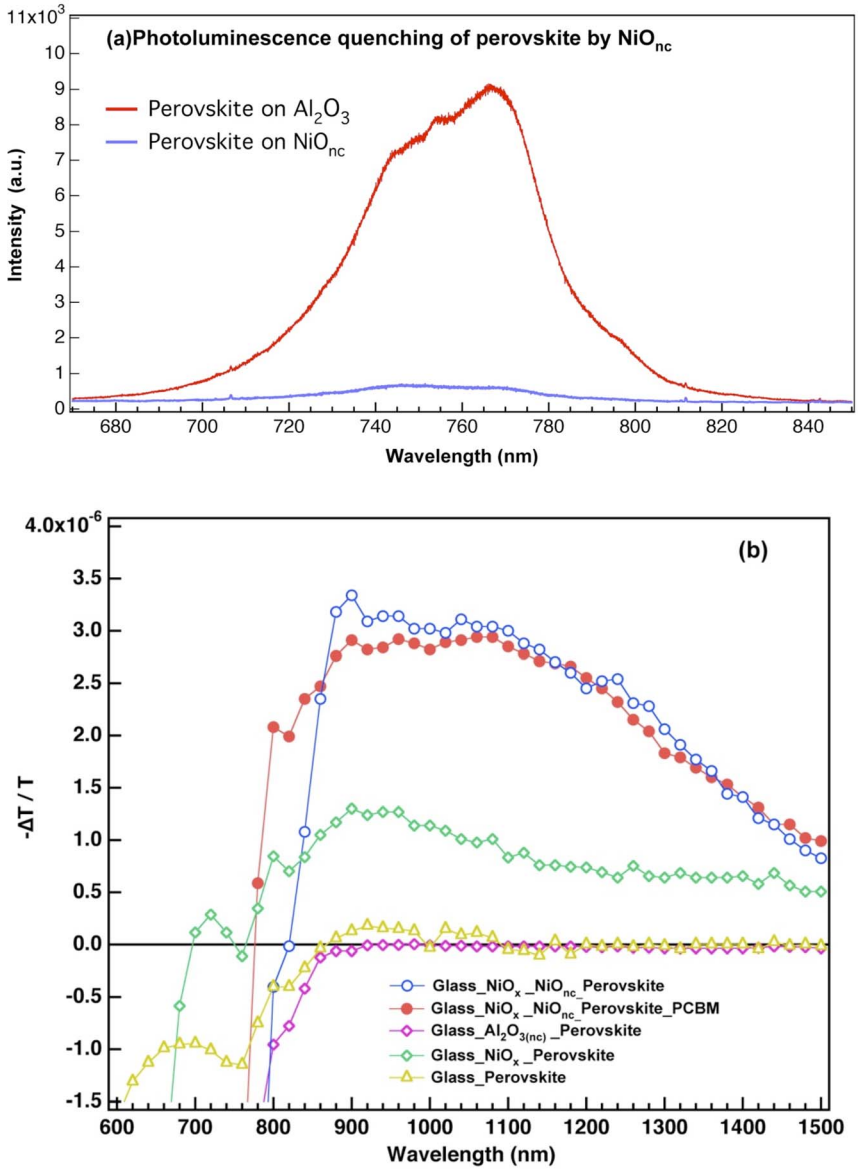

Figure 4 | The photoluminescence (PL) spectra (a) and photoinduced transient absorption spectra (b) of perovskite coated on various substrates. In (a), the red line presents the PL of perovskite coated on mesoscopic Al_2O_3 nanoparticles, and the blue line of perovskite coated on NiO_{nc}. In (b), NiO_x denotes the planar spin coated thin film, NiO_{nc} means the mesoscopic NiO nanocrystalline thin film and $Al_2O_{3(nc)}$ refers to mesoscopic Al_2O_3 nanocrystalline thin film.

examine the quenching of the perovskite in junction with various contact materials[8]. Recent results on quenching of PL in the composite perovskite films showed that PCBM is a very efficient n-type quencher while Spiro-OMeTAD, PEDOT:PSS, V_2O_5, NiO and P3HT are efficient p-type counterparts[8,28]. The NiO/perovskite film was observed with a very high yield (95%) of PL quenching but a well-performed device was not developed due to poor surface coverage and morphological control for the formation of uniform perovskite layer on NiO_x film[8]. Our approach of using a mesoscopic NiO_{nc} layer provided a mesoporous matrix for sufficient loading of the perovskite material and lowered the demand for control of morphology as for the PHJ. To further confirm the carrier separation phenomenon, we performed the photo-induced transient absorption (PIA) measurement to examine the signature of long-lived charge separation species between various junctions. PIA spectra of the samples containing film configurations of G/P, G/Al_2O_3/P, G/NiO/P and G/NiO/P/PC_{61}BM (G stands for glass and P for perovskite) were carried out in the spectral range between 600 ~ 1500 nm at the excitation wavelength of 460 nm, and the results are shown in Fig. 4(b). The PIA spectra of the G/P (brown) and G/Al_2O_3/P (purple) films show only the negative signals in the spectral region below 800 nm representing the characteristics of the absorption and emission of the perovskite species. In contrast, the PIA spectra of the G/NiO/P (blue for NiO_x/NiO_{nc} and green for NiO_x substrate) film show a broad spectral feature above 800 nm which we assigned to the long-lived charge-separation state of NiO^+/P^-. The PIA signal in the NiO_x/$NiO_{(nc)}$ film was much greater than that in the NiO_x/P film indicating that the NiO^+ species was produced in a larger extent for the former than for the latter. The oxidized NiO species has been observed in the electrochemical spectrum of nanostructured NiO featuring a broad range of absorption in the infrared region which corresponds to our PIA feature[48]. For the G/NiO/P/PC_{61}BM (red) film containing the electron-accepting layer, the PIA spectrum was quite similar to that of G/NiO/P film in the spectral range 900 ~ 1500 nm. Since PCBM has been verified to be an effective electron acceptor in perovskite/PCBM junction[8,9,15,16,22,49,50], the above evidence confirms that the observed broad absorption band is mainly due to the formation of the NiO^+ cationic species upon photo excitation of the perovskite/NiO film at 460 nm. The PIA results revealed that the charge separation at the interface between perovskite and NiO is viable so that the resulting perovskite in our device is sandwiched between two efficient selective contacts that facilitate charge extraction featuring very high V_{OC} and great device performance. Further investigations on ultrafast relaxation and carrier dynamics in the NiO/perovskite interface are underway to understand the underlying charge transport kinetics governing the operation of this type of solar cells.

Many efforts have been contributed to improve the device performance for p-type sensitized solar cells. The state-of-the-art p-type DSCs delivered less than 1.5% PCE[37,38,40]. The reasons for this much lower photovoltaic action compared with its n-type sensitization counterpart have been ascribed to the fast recombination, short hole diffusion length in p-type semiconductor and unfavorable redox energy levels of electrolyte with respect to the p-type metal oxide valence band[40,51]. The performance of the solar device described in this article greatly outperformed the conventional p-type sensitized solar cells or other p-type oxide semiconductor heterojunction solar cells. The success of such highly efficient p-type metal oxide heterojunction solar cells is vital for the future development of fully inorganic perovskite-based solar cells as well as the tandem devices.

Our results strongly confirmed the functionality of p-type NiO metal oxide acting as a selective contact is feasible. The future perspective is to integrate n-type contact material for the construction of a fully inorganic p-i-n heterojunction solar cell with perovskite absorber sandwiched between two wide band gap oxide semiconductors. This offers a configuration of superior thin film (or super mesoscopic) photovoltaic device using robust and extreme thin photoactive material. Additionally, our device provided a base for the tandem architecture or p-n dual sensitization photovoltaic. It would be crucial to explore low temperature process for metal oxide deposition and to introduce interconnection transparent connection layer for tandem cells. These topics are currently the subjects of research focuses in our group.

In conclusion, a methylammonium lead iodide ($CH_3NH_3PbI_3$) perovskite/NiO heterojunction solar cell is developed to achieve remarkable efficiency of 9.51% of power conversion efficiency. This is the first demonstration of a p-type mesoscopic metal oxide as an efficient hole collecting contact. The success of this heterojunction will provide varieties for cell design and the realization of fully inorganic mesoscopic solar cells since the organic p-contact widely used in the past can now be replaced by the robust wide band gap metal oxide reported herein. It is expected that the device stability could be improved significantly with the application of metal oxide selective contact materials. We believe that further efforts can be made on the material optimization and judicious selection of contact materials, and robust device or tandem configuration could be achieved for perovskite-based solar cells.

Methods

Fabrication of NiO_x solution. The precursor for NiO_x film coating was prepared with 0.5 M nickel formate dihydrate (Alfa Aesar) in ethylene glycol solution containing 1 M ethylenediamine (Aldrich) and filtered with 0.45 μm nylon filters[41].

Fabrication of NiO_{nc} paste. The mesoporous NiO solution used for spin coating was prepared by diluting slurry NiO with anhydrous ethanol in a ratio of 1 : 7. Slurry NiO was prepared by mixing 3 g of NiO nanopowder (Inframat) in 80 ml ethanol and subsequently adding with 15 g of 10 wt% ethyl cellulose (in EtOH) and 10 g of terpineol. The solution was stirred and dispersed with ultrasonic horn and concentrated with rotary evaporator for ethanol removal until 23 mbar.

Fabrication of CH_3NH_3I. CH_3NH_3I was synthesized as our previous literature. Methylamine (CH_3NH_2) (13.5 mL, 40 wt% in aqueous solution, Alfa Aesar) and hydroiodic acid (HI) (15.0 mL, 57 wt% in water, Alfa Aesar) were stirred at 0°C under nitrogen atmosphere for 2 h. After the reaction, the solvent of the solution was evaporated using a rotary evaporator. A white powder, methyl ammonium iodide (CH_3NH_3I), was generated by the reaction. The precipitate was washed with diethyl ether (Sigma–Aldrich) three times and dried at 60°C in a vacuum oven overnight[1,3,7,25].

Device fabrication. The device fabrication was similar to our previous published procedure[7,43]. Patterned ITO-coated glass substrates (Ritek Corp., 15 Ω/sq.) are ultrasonically cleaned with soap water, deionized water and ethanol. Then, the substrates are rinsed with 2-propanol and Acetone, followed by UV-Ozone cleaner (Model: 42, Jelight, USA) treatment for 25 minutes. NiO_x electrode-interlayer, using solution synthesized as described previously, was spun-cast onto the substrates at 4000 rpm for 90 s using spin-coater, and then annealed at 300°C for 1 hour. After NiO_x film was cooled to room temperature, the substrates are spin-coated with $NiO_{(nc)}$ at 4000 rpm for 30 seconds. After being annealed at 400°C for 30 minutes, the resulting films will form mesoporous NiO film. $CH_3NH_3PbI_3$ is deposited on NiO_x by one step spin coating[43] (9500 rpm for PHJ device) or sequential deposition method on mesoporous NiO_{nc} film (mesoscopic devices) with procedures referred to reported literature[11]. In order to have PbI_2 solution (1 M in N,N-dimethylformamide) uniformly deposited well in the mesoscopic pore, the substrates are preheated at 70°C prior to the deposition of PbI_2. PbI_2 solution is spun onto the mesoporous NiO_{nc} film at 6500 rpm for 5 seconds, followed by annealing at 70°C for 30 minutes. After cooling to room temperature, the resulting films are immersed into 2-propanol to pre-wet the substrates and then dipped into a solution of CH_3NH_3I (10 mg/ml in 2-propanol) for 40 seconds at room temperature, and then annealed at 70°C for 30 minutes. The color of the resulting films becomes dark brown from bright yellow. $PC_{61}BM$ or $PC_{71}BM$ (20 ~ 25 nm) (> 99%, Solenne, Netherlands), BCP (10 nm) (Aldrich), and Al (100 nm) were thermally deposited on the substrate inside a vacuum chamber (10^{-6} Torr). The deposition thickness was monitored by the quartz crystal balance. The active area of the device is 0.06 cm^2. All the procedures are implemented inside a nitrogen-filled glove box with oxygen and moisture levels < 1 ppm except for fabrication of NiO_x electrode-interlayer and mesoporous NiO_{nc} film.

Absorbance and Light Harvesting Efficiency (LHE). The UV-vis spectra were measured by a spectrometer (U-4100, Hitachi). The samples for the optical characterization of perovskite are deposited on ITO/NiO_x (spin coated at 9500 rpm) and ITO/NiO_x/NiO_{nc} (sequential deposition) substrates for planar and mesoscopic thin film respectively. The substrates are taken as baseline for the measurements.

Photoluminescence spectroscopy. Room-temperature micro-photoluminescence measurements were performed using the He–Cd laser at 325 nm with optical power of 7 mW. A NUV 40× objective lens was used for the collection of the pump light and the emitted light from the sample. The emission was dispersed by a 0.32 m focal length spectrometer with 1800 grooves/mm and detected by Liquid N2-cooled charged couple device (CCD) detector.

Photo-induced transient absorption. Excitation of the thin-film samples was achieved by a cw laser at 460 nm and modulated with a chopper (Thorlab, MC2000) at 19 Hz. The light source of the absorption spectra was provided by a Xenon lamp (PTi A-1010, 150 W) coupled with a monochromator (Acton Research Corporation, SpectraPro-300i). The PIA signals were obtained with a lock-in amplifier (Stanford Research System, SR830) via two detectors – Si photodiode (Thorlab, DET100) in the visible/NIR region (600–900 nm) and Ge detector (Thorlab, DET50B) in the NIR region (800–1500 nm). All the PIA measurements were performed right after the samples were prepared.

1. Kojima, A., Teshima, K., Shirai, Y. & Miyasaka, T. Organometal Halide Perovskites as Visible-Light Sensitizers for Photovoltaic Cells. *J. Am. Chem. Soc.* **131**, 6050–6051 (2009).
2. Im, J.-H., Lee, C.-R., Lee, J.-W., Park, S.-W. & Park, N.-G. 6.5% efficient perovskite quantum-dot-sensitized solar cell. *Nanoscale* **3**, 4088–4093 (2011).
3. Kim, H.-S. *et al.* Lead Iodide Perovskite Sensitized All-Solid-State Submicron Thin Film Mesoscopic Solar Cell with Efficiency Exceeding 9%. *Sci. Rep.* **2**, 591 (2012).
4. Lee, M. M., Teuscher, J., Miyasaka, T., Murakami, T. N. & Snaith, H. J. Efficient Hybrid Solar Cells Based on Meso-Superstructured Organometal Halide Perovskites. *Science* **338**, 643–647 (2012).
5. Noh, J. H., Im, S. H., Heo, J. H., Mandal, T. N. & Seok, S. I. Chemical Management for Colorful, Efficient, and Stable Inorganic–Organic Hybrid Nanostructured Solar Cells. *Nano Lett.* **13**, 1764–1769 (2013).
6. Snaith, H. J. Perovskites: The Emergence of a New Era for Low-Cost, High-Efficiency Solar Cells. *J. Phys. Chem. Lett.* **4**, 3623–3630 (2013).
7. Jeng, J.-Y. *et al.* CH3NH3PbI3 Perovskite/Fullerene Planar-Heterojunction Hybrid Solar Cells. *Adv. Mater.* **25**, 3727–3732 (2013).
8. Docampo, P., Ball, J. M., Darwich, M., Eperon, G. E. & Snaith, H. J. Efficient organometal trihalide perovskite planar-heterojunction solar cells on flexible polymer substrates. *Nat Commun* **4**, 2761 (2013).
9. Sun, S. *et al.* The origin of high efficiency in low-temperature solution-processable bilayer organometal halide hybrid solar cells. *Energy Environ. Sci.* **7**, 399–407 (2014).
10. Ku, Z., Rong, Y., Xu, M., Liu, T. & Han, H. Full Printable Processed Mesoscopic CH3NH3PbI3/TiO2 Heterojunction Solar Cells with Carbon Counter Electrode. *Sci. Rep.* **3**, 3132 (2013).
11. Burschka, J. *et al.* Sequential deposition as a route to high-performance perovskite-sensitized solar cells. *Nature* **499**, 316–319 (2013).
12. Liu, M., Johnston, M. B. & Snaith, H. J. Efficient planar heterojunction perovskite solar cells by vapour deposition. *Nature* **501**, 395–398 (2013).
13. Liu, D. & Kelly, T. L. Perovskite solar cells with a planar heterojunction structure prepared using room-temperature solution processing techniques. *Nature Photon.* **8**, 133–138 (2014).
14. Park, N.-G. Organometal Perovskite Light Absorbers Toward a 20% Efficiency Low-Cost Solid-State Mesoscopic Solar Cell. *J. Phys. Chem. Lett.* **4**, 2423–2427 (2013).
15. Stranks, S. D. *et al.* Electron-Hole Diffusion Lengths Exceeding 1 Micrometer in an Organometal Trihalide Perovskite Absorber. *Science* **342**, 341–344 (2013).
16. Xing, G. *et al.* Long-Range Balanced Electron- and Hole-Transport Lengths in Organic-Inorganic CH3NH3PbI3. *Science* **342**, 344–347 (2013).
17. Gonzalez-Pedro, V. *et al.* General Working Principles of CH3NH3PbX3 Perovskite Solar Cells. *Nano Lett.* **14**, 888–893 (2014).
18. Heo, J. H. *et al.* Efficient inorganic-organic hybrid heterojunction solar cells containing perovskite compound and polymeric hole conductors. *Nature Photon.* **7**, 487–492 (2013).
19. Kumar, M. H. *et al.* Flexible, low-temperature, solution processed ZnO-based perovskite solid state solar cells. *Chem. Comm.* **49**, 11089–11091 (2013).
20. Eperon, G. E., Burlakov, V. M., Docampo, P., Goriely, A. & Snaith, H. J. Morphological Control for High Performance, Solution- Processed Planar Heterojunction Perovskite Solar Cells. *Adv. Funct. Mater.* **24**, 151–157 (2014).
21. Chen, Q. *et al.* Planar Heterojunction Perovskite Solar Cells via Vapor-Assisted Solution Process. *J. Am. Chem. Soc.* (2013).
22. Malinkiewicz, O. *et al.* Perovskite solar cells employing organic charge-transport layers. *Nature Photon.* **8**, 128–132 (2014).
23. Qiu, J. *et al.* All-solid-state hybrid solar cells based on a new organometal halide perovskite sensitizer and one-dimensional TiO2 nanowire arrays. *Nanoscale* **5**, 3245–3248 (2013).
24. Kim, H.-S. *et al.* High Efficiency Solid-State Sensitized Solar Cell-Based on Submicrometer Rutile TiO2 Nanorod and CH3NH3PbI3 Perovskite Sensitizer. *Nano Lett.* **13**, 2412–2417 (2013).
25. Etgar, L. *et al.* Mesoscopic CH3NH3PbI3/TiO2 Heterojunction Solar Cells. *J. Am. Chem. Soc.* **134**, 17396–17399 (2012).
26. Laban, W. A. & Etgar, L. Depleted hole conductor-free lead halide iodide heterojunction solar cells. *Energy Environ. Sci.* **6**, 3249–3253 (2013).
27. Bi, D. *et al.* Efficient and stable CH3NH3PbI3-sensitized ZnO nanorod array solid-state solar cells. *Nanoscale* **5**, 11686–11691 (2013).
28. Conings, B. *et al. Perovskite-Based Hybrid Solar Cells Exceeding 10% Efficiency with High Reproducibility Using a Thin Film Sandwich Approach. Adv. Mater., DOI: 10.1002/adma.201304803* (2013).
29. Cai, B., Xing, Y., Yang, Z., Zhang, W.-H. & Qiu, J. High performance hybrid solar cells sensitized by organolead halide perovskites. *Energy Environ. Sci.* **6**, 1480–1485 (2013).
30. Abrusci, A. *et al.* High-Performance Perovskite-Polymer Hybrid Solar Cells via Electronic Coupling with Fullerene Monolayers. *Nano Lett.* **13**, 3124–3128 (2013).
31. Noh, J. H. *et al.* Nanostructured TiO2/CH3NH3PbI3 heterojunction solar cells employing spiro-OMeTAD/Co-complex as hole-transporting material. *J. Mater. Chem. A* **1**, 11842–11847 (2013).
32. Jeon, N. J. *et al.* Efficient Inorganic–Organic Hybrid Perovskite Solar Cells Based on Pyrene Arylamine Derivatives as Hole-Transporting Materials. *J. Am. Chem. Soc.* **135**, 19087–19090 (2013).
33. Di Giacomo, F. *et al.* High efficiency CH3NH3PbI(3−x)Clx perovskite solar cells with poly(3-hexylthiophene) hole transport layer. *J. Power Sources* **251**, 152–156 (2014).
34. Christians, J. A., Fung, R. C. M. & Kamat, P. V. An Inorganic Hole Conductor for Organo-Lead Halide Perovskite Solar Cells. Improved Hole Conductivity with Copper Iodide. *J. Am. Chem. Soc.* **136**, 758–764 (2014).
35. Irwin, M. D., Buchholz, D. B., Hains, A. W., Chang, R. P. H. & Marks, T. J. p-Type semiconducting nickel oxide as an efficiency-enhancing anode interfacial layer in polymer bulk-heterojunction solar cells. *PNAS* **105**, 2783–2787 (2008).
36. Nattestad, A. *et al.* Highly efficient photocathodes for dye-sensitized tandem solar cells. *Nature Mater.* **9**, 31–35 (2010).
37. Powar, S. *et al.* Highly Efficient p-Type Dye-Sensitized Solar Cells based on Tris(1,2-diaminoethane)Cobalt(II)/(III) Electrolytes. *Angew. Chem. Int. Ed.* **52**, 602–605 (2013).
38. Gibson, E. A. *et al.* A p-Type NiO-Based Dye-Sensitized Solar Cell with an Open-Circuit Voltage of 0.35 V. *Angew. Chem. Int. Ed.* **48**, 4402–4405 (2009).
39. Ratcliff, E. L. *et al.* Investigating the Influence of Interfacial Contact Properties on Open Circuit Voltages in Organic Photovoltaic Performance: Work Function Versus Selectivity. *Adv. Energy Mater.* **3**, 647–656 (2013).
40. Odobel, F. & Pellegrin, Y. Recent Advances in the Sensitization of Wide-Band-Gap Nanostructured p-Type Semiconductors. Photovoltaic and Photocatalytic Applications. *J. Phys. Chem. Lett.* **4**, 2551–2564 (2013).
41. Garcia, A. *et al.* Improvement of Interfacial Contacts for New Small- Molecule Bulk-Heterojunction Organic Photovoltaics. *Adv. Mater.* **24**, 5368–5373 (2012).
42. Manders, J. R. *et al.* Solution-Processed Nickel Oxide Hole Transport Layers in High Efficiency Polymer Photovoltaic Cells. *Adv. Funct. Mater.* **23**, 2993–3001 (2013).
43. Jeng, J.-Y. *et al. Nickel Oxide Electrode Interlayer in CH3NH3PbI3 Perovskite/PCBM Planar-Heterojunction Hybrid Solar Cells. Adv. Mater. DOI:10.1002/adma.201306217* (2014).
44. Mühlbacher, D. *et al.* High Photovoltaic Performance of a Low-Bandgap Polymer. *Adv. Mater.* **18**, 2884–2889 (2006).
45. Wienk, M. M., Turbiez, M., Gilot, J. & Janssen, R. A. J. Narrow-Bandgap Diketo-Pyrrolo-Pyrrole Polymer Solar Cells: The Effect of Processing on the Performance. *Adv. Mater.* **20**, 2556–2560 (2008).
46. Liang, Y. *et al.* Development of New Semiconducting Polymers for High Performance Solar Cells. *J. Am. Chem. Soc.* **131**, 56–57 (2008).
47. Huang, F. *et al.* Development of New Conjugated Polymers with Donor−π-Bridge−Acceptor Side Chains for High Performance Solar Cells. *J. Am. Chem. Soc.* **131**, 13886–13887 (2009).
48. Boschloo, G. & Hagfeldt, A. Spectroelectrochemistry of Nanostructured NiO. *J. Phys. Chem. B* **105**, 3039–3044 (2001).
49. You, J. *et al.* Low-Temperature Solution-Processed Perovskite Solar Cells with High Efficiency and Flexibility. *Acs Nano* **8**, 1674–1680 (2014).
50. Chiang, Y.-F. *et al.* High voltage and efficient bilayer heterojunction solar cells based on organic-inorganic hybrid perovskite absorber with low-cost flexible substrate. *Phys. Chem. Chem. Phys.* **16**, 6033–6040 (2014).
51. Borgström, M. *et al.* Sensitized Hole Injection of Phosphorus Porphyrin into NiO: Toward New Photovoltaic Devices. *J. Phys. Chem. B* **109**, 22928–22934 (2005).

Acknowledgments

P.C. appreciates the research funding from National Science Council (NSC) of Taiwan (NSC102-2113-M-006-010). T.F.G. would like to thank the NSC of Taiwan (NSC102-2682-M-006-001-MY3) for financially supporting this research. E.W.G.D. acknowledges the support from NSC of Taiwan (NSC102-2113-M- 009-020-MY3).

Author contributions

P.C. and T.-F.G. both proposed the research and supervised the whole project. K.-C.W., J.-Y.J. and P.-S.S. carried out the experiments for device fabrication, optimization and

characterizations. P.C., T.-F.G. and E.W.-G.D. contributed to the data analysis and interpretation for the results. K.-C.W. performed the HR-SEM measurements. C.-H.T., T.-Y.C. and H.-C.H. measured the PL spectra. P.-Y.L. prepare the NiO_x and perovskite precursor materials. E.W.-G.D. supervised the PIA measurements while Y.-C.C. conducted the experiments. T.-C.W. supervised the preparation of materials and participated the discussion. P.C. wrote the manuscript with further inputs from all the other authors.

Additional information

Supplementary information accompanies this paper at http://www.nature.com/scientificreports

Competing financial interests: The authors declare no competing financial interests.

How to cite this article: Wang, K.-C. *et al*. p-type Mesoscopic Nickel Oxide/Organometallic Perovskite Heterojunction Solar Cells. *Sci. Rep.* **4**, 4756; DOI:10.1038/srep04756 (2014).